

Zero-Shot Coreset Selection: Efficient Pruning for Unlabeled Data

Brent A. Griffin¹ Jacob Marks¹ Jason J. Corso^{1,2}
¹ Voxel51 ² University of Michigan
 {brent, jacob, jason}@voxel51.com

Abstract

Deep learning increasingly relies on massive data with substantial costs for storage, annotation, and model training. To reduce these costs, coreset selection aims to find a representative subset of data to train models while ideally performing on par with the full data training. State-of-the-art coreset methods use carefully-designed criteria to quantify the importance of each data example via ground truth labels and dataset-specific training, then select examples whose scores lie in a certain range to construct a coreset. These methods work well in their respective settings, however, they cannot select data that are unlabeled, which is the majority of real-world data. To that end, this paper motivates and formalizes the problem of unlabeled coreset selection to enable greater scale and reduce annotation costs for deep learning. As a solution, we develop **Zero-Shot Coreset Selection (ZCore)**, a method that efficiently selects coresets without ground truth labels or training on candidate data. Instead, ZCore uses existing foundation models to generate a zero-shot embedding space for unlabeled data, then quantifies the relative importance of each example based on overall coverage and redundancy within the embedding distribution. We evaluate ZCore on four datasets and outperform several state-of-the-art label-based methods, leading to a strong baseline for future research in unlabeled coreset selection. On ImageNet, ZCore selections achieve a downstream model accuracy of 53.99% with only 10% training data, which outperforms label-based methods while removing annotation requirements for 1.15 million images. Our code is publicly available at <https://github.com/voxel51/zcore>.

1. Introduction

The computational cost to train a single state-of-the-art deep learning model in various fields doubles every 3.4 months in the deep learning era due to increasingly large models and datasets [1, 46]. Since the introduction of AlexNet [18], groundbreaking models in computer vision like ViT and DALL-E all rely on massive datasets for training [10, 32].

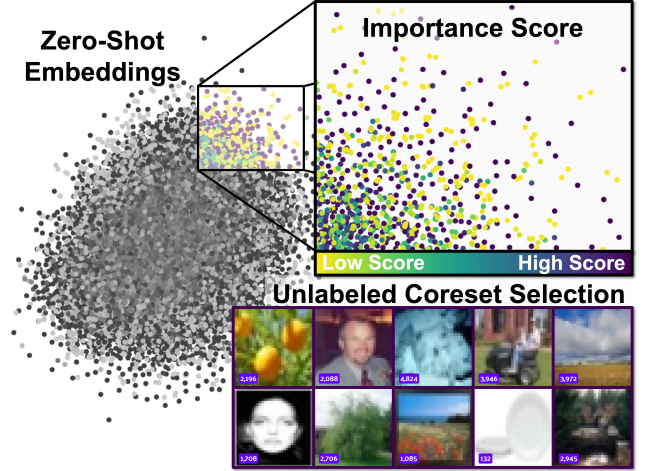


Figure 1. **Zero-Shot Coreset Selection Overview.** We select coresets from previously unseen and unlabeled data by first using foundation models to generate a dataset embedding space representation (e.g., a 2-D slice of CLIP on CIFAR100, left). Second, we use the embeddings to calculate an importance score that rewards examples individually covering large portions of the embedding space while penalizing neighbors to remove redundancy (right, top). Finally, we output a coreset of examples for any given prune rate using the score rank (right, bottom). Embeddings and data visualizations generated using the FiftyOne Library [24].

However, there are substantial costs to collecting, storing, transmitting, and pre-processing such a vast amount of data. Furthermore, training models on vast datasets introduces yet another substantial cost for computation, sometimes hundreds of thousands of GPU hours to achieve satisfactory performance, which frustrates applications requiring repeat training over datasets such as hyperparameter optimization [20, 21] and neural architecture search [11, 19].

Coreset selection deals with large data to mitigate the above issues for data-efficient deep learning. Specifically, coreset selection reduces the training set size by selecting a pruned subset that contains only valuable examples (the *core set*), such that models trained on the coreset achieve similar performance to those trained on the original, full dataset [12]. Several recent works provide various coreset selection methods using carefully-designed criteria, includ-

ing median class values [41], diverse coverage of importance scores [48], and gradient dynamics during training [44], which achieves 53.91% accuracy on ImageNet with only 10% training data.

State-of-the-art coreset selection methods have demonstrated impressive results in experiment settings. However, the current SOTA methods assume the full dataset is labeled and available for training prior to coreset selection. Regarding labels, it is important to acknowledge that the majority of real-world data are, in fact, unlabeled, preventing coreset selection from label-based methods. Furthermore, labeling massive amounts of image data just to consider selection is cost prohibitive, with annotation taking anywhere between 7 seconds per bounding box to 1.5 hours for full semantic segmentation [8, 16]. Some innovative coreset selection methods use self-supervised learning in place of label-based training [35]; however, this approach will still have substantial time and computation costs to select coresets at scale. Furthermore, coupling coreset selection with training on a single model architecture decreases generalization.

To that end, this paper addresses the problem of coreset selection without labels or training using a novel approach. First, we formulate the problem of unlabeled coreset selection, which reduces data- and label-based costs by generating coresets from unlabeled data. After coreset selection from the larger dataset, labels are *only* used by the actual model to train on the pruned dataset. Notably, if coreset selections are for self-supervised training, no labels are used. Second, we use the unlabeled coreset selection formulation to develop Zero-Shot Coreset Selection (ZCore), a method which *also* reduces computation costs by selecting coresets without training on the candidate dataset. Instead, ZCore uses foundation models off-the-shelf to generate a candidate selection embedding space, which is then iteratively sampled and scored to estimate the value of each example’s value based on coverage of the embedding space and redundancy within the coreset (see Fig. 1). Our contributions are:

1. We motivate and formalize the problem of unlabeled coreset selection, which substantially reduces data- and label-based costs for efficient deep learning at scale.
2. We develop our Zero-Shot Coreset Selection method (ZCore), which is computationally efficient and uses novel estimates of dataset distribution coverage and redundancy to select coresets from larger, unlabeled datasets, enabling broader use of coreset selection.
3. We evaluate ZCore against state-of-the-art label- and training-based coreset selection methods with eight baselines on four different datasets spanning three orders of magnitude for scale. Results show that our method performs best in multiple cases and overall outperforms all label-based methods save one, while reducing label and computation costs.

From these results, ZCore establishes a new state-of-the-art.

2. Related Work

Dataset Distillation is similar to coreset selection in that it comprises many innovative methods for data-efficient deep learning. On a functional level, the objectives of many coreset methods also apply to dataset distillation, however, as opposed to selecting a subset of *existing* data for a coreset, dataset distillation aims to generate a much smaller dataset with *synthetic* examples that yield the same performance as the larger initial dataset [43]. Notable dataset distillation methods generate synthetic examples relative to the initial dataset by matching gradients [47], differentiable Siamese augmentation for better synthesis [45], aligning features [38], multi-step parameter matching [5], and embedding space distribution matching [46]. These dataset distillation methods are remarkable for their creation of small but effective synthetic training datasets. On the other hand, our current work focuses on evaluating and selecting coresets from existing real-world data.

Active Learning is another active research area with many contributions to data-efficient deep learning. The goal of active learning is to enable learning algorithms to perform better with less training by letting them choose their own data [34], which is especially useful in cases where large portions of data are unlabeled and manual labeling is expensive [4]. In fact, active learning encompasses the particularly hard problem of starting selection with no initial labeled examples, i.e., the cold start problem [22]. Notably, some recent active learning methods focus on the importance of coverage diversity in data selection [2, 6]. However, these methods actively train and select data on an increasing set for a specific model, which is not conducive for *model-agnostic, one-shot* coreset selection.

Coreset Selection prunes datasets down to a smaller, valuable *core set* to reduce costs and enable more data-efficient deep learning. A basic solution to find the optimal coreset is to search through and train on every subset to find the best corresponding model performance. However, this simple approach is NP-hard, which has led to the development of many innovative coreset selection methods. Early coreset methods generally expect a consistent data distribution to the original dataset [3, 12], e.g., [40] greedily adds one sample at a time to match embedding space centers. Other coreset methods can be broadly categorized as selecting by optimization [39, 42], coverage or diversity [33, 48], and importance criteria [36, 37]. Recent coreset innovations address ongoing challenges such as application on a wide range of dataset sizes [41], making selections on data with label errors [26], and fully utilizing training dynamics [44].

Our current work is inspired by the success of this previous coreset selection work. However, a drawback for current state-of-the-art coreset selection methods is requiring labels and/or training on the larger initial dataset (see Tab. 1). Thus, in this paper, we focus on extending core-

Table 1. Comparison of data and **procedural requirements** across coreset selection methods.

Methods	Selects Coreset Data		
	<i>without Training on Data</i>	<i>without Ground Truth Labels</i>	<i>without Prune Specific Tuning</i>
Zero-Shot Coreset Selection (ours), Random	Yes	Yes	Yes
Self-Supervised Selection [35] NeurIPS 2022	No	Yes	Yes
Dyn-Unc [14] CVPR WS '24, Moderate [41] ICLR 2023	No	No	Yes
TDDS [44] CVPR 2024, Coverage [48] ICLR 2023	No	No	No

set selection to unlabeled data without any requirements for dataset- or architecture-specific training. This extends applicability to new data and models while reducing costs associated with annotating data with ground truth labels, sensitivity to label errors, and extensive computation at scale.

3. Unlabeled Coreset Selection

We first define the problem of *labeled* coreset selection for data-efficient deep learning. Formally, we are given a labeled dataset $\mathbb{S}^l = \{(\mathbf{x}_i, y_i)\}_{i=1}^N$ with N examples drawn i.i.d. from an underlying distribution P , where \mathbf{x}_i are the data and y_i is the ground truth label for each example. The goal is to select a subset of \mathbb{S}^l to reduce future storage and training consumption while closely maintaining performance of full dataset training. We denote this *coreset* as $\mathbb{S}^c = \{(\mathbf{x}_i, y_i)\}_{i=1}^n \subset \mathbb{S}^l$, which has n examples and a *prune rate* of $1 - \frac{n}{N}$. We formulate coreset selection as [33]:

$$\arg \min_{\mathbb{S}^c \subset \mathbb{S}^l | 1 - \frac{n}{N} \geq p} \mathbb{E}_{\mathbf{x}, y \sim P} [l(\mathbf{x}, y; f_{(\mathbb{S}^c)})], \quad (1)$$

where p is a prune rate set *before* training, l is the loss function, and $f_{(\mathbb{S}^c)}$ is a model trained on \mathbb{S}^c . Notably, many SOTA methods select \mathbb{S}^c by assigning an importance score to each example (e.g., [44]). For later use, we denote the importance score as $s \in \mathbb{R}^N$.

We now define the problem of *unlabeled* coreset selection for data- and *label*-efficient deep learning. Formally, given an unlabeled dataset $\mathbb{S} = \{\mathbf{x}_i\}_{i=1}^N$, the goal is to select $\mathbb{S}^c \subset \mathbb{S}$ without using *any* ground-truth label y_i . The motivation for this change is that it is preventative to label an entire massive dataset when much of the data will be pruned. We formulate unlabeled coreset selection by replacing $\mathbb{S}^c \subset \mathbb{S}^l$ with $\mathbb{S}^c \subset \mathbb{S}$ in Eq. (1). Notably, after selecting \mathbb{S}^c , we add n labels to the coreset as $\mathbb{S}^c = \{(\mathbf{x}_i, y_i)\}_{i=1}^n$ *only* to train the pruned model $f_{(\mathbb{S}^c)}$.

Along with the aforementioned benefits of coreset selection, unlabeled coreset selection uniquely increases scale and reduces labeling costs. First, while we can use any \mathbf{x}_i from a labeled dataset \mathbb{S}^l , we can also extensively sample and consider more examples \mathbf{x} from the underlying distribution P without any annotation or labeling requirements.

This extension enables us to source coresets from a much larger initial dataset. In effect, unlabeled coreset selection extends dataset pruning to the majority of unlabeled, real-world data. Second, we only label the n coreset examples after they are selected for pruned model training, so there is a $N - n$ reduction in labeling costs relative to label-based selection. On ImageNet, unlabeled selection at a 90% prune rate removes label requirements for 1.15 million images.

4. Zero-Shot Coreset Selection

We use the unlabeled coreset selection formulation to develop a new method of “Zero-Shot” Coreset Selection (ZCore). In place of label- or training-based selection, ZCore instead uses foundation models to generate a zero-shot embedding space representation of the initial dataset (Sec. 4.1). ZCore then samples the embedding space to determine which examples provide valuable coverage (Sec. 4.2). Subsequently, ZCore determines which examples in proximity to those providing coverage are redundant (Sec. 4.3). Finally, ZCore uses the coverage and redundancy metrics to iteratively sample and score each candidate training example to determine final coreset selections (Sec. 4.4).

4.1. Foundational Embedding Representation

ZCore uses a zero-shot embedding space representation of unlabeled dataset \mathbb{S} to select data. We generate embeddings using a foundation model denoted as $f(\cdot) = g(h(\cdot))$, where h is the model component mapping input data to hidden representations at the penultimate layer and g maps the embedding space to a previously learned output f . We use $h(\mathbf{x}_i) \in \mathbb{R}^M$ to generate an M -dimension *embedding space* for input data $\mathbb{S} = \{\mathbf{x}_i\}_{i=1}^N$ denoted as

$$\mathbf{Z} = [h(\mathbf{x}_1), \dots, h(\mathbf{x}_N)] \in \mathbb{R}^{N \times M}. \quad (2)$$

Embedding space \mathbf{Z} lets us to use the previously learned hidden representation of h as a zero-shot alternative to label- or training-based coreset selection. In general, examples corresponding to different classes or concepts map to different regions of the feature-based embedding space. Thus, we quantify the importance of each example in terms of relative coverage and redundancy in \mathbf{Z} as a representation of the underlying data distribution $\mathbf{x}, y \sim P$ in Eq. (1).

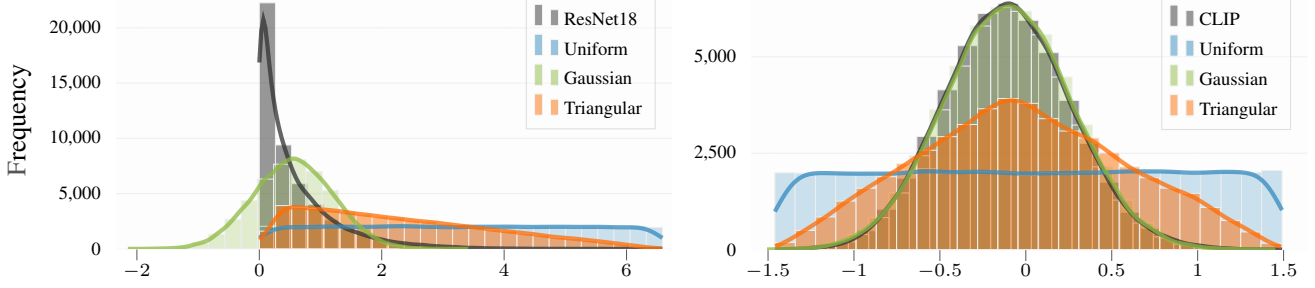


Figure 2. Comparison of real embedding data (gray) and **sampling techniques**. ResNet18 (left) and CLIP (right) are the first dimension embeddings for 50,000 CIFAR100 train set examples, while each corresponding distribution type is sampled 50,000 times. Relative to uniform or Gaussian, our Triangular distribution uniquely achieves all objectives of: providing sufficient coverage for densely populated regions of the embedding space, covering outliers, and not oversampling empty space.

Remarks on \mathbf{Z} : In Sec. 5 experiments, we generate all model embeddings in advance using off-the-shelf weights for a ResNet18 [13] and CLIP ViT-L-14 model [31], which we concatenate as $h(\mathbf{x}_i) = \begin{bmatrix} h^{\text{RN18}}(\mathbf{x}_i) \\ h^{\text{CLIP}}(\mathbf{x}_i) \end{bmatrix} \in \mathbb{R}^{1,280}$. Relative to coreset methods using full dataset training for 60-200 epochs, generating embeddings takes less time than one train epoch because it only requires one forward pass per sample, a subcomponent of the full model architecture (h), and no training-based back propagation or metric tracking.

4.2. Coverage of the Embedding Space

Our first objective for coreset selection is to select examples that maximize coverage of embedding space \mathbf{Z} . To quantify coverage, we develop a Monte Carlo-inspired sampling technique [23], which estimates the relative contribution of each candidate training example $\mathbf{x}_i \in \mathbb{S}$ in covering a carefully designed distribution over the embedding space.

We assume a Triangular distribution over each embedding space dimension $j \in \{1, \dots, M\}$ using

$$z_j \sim p(x, j) := \begin{cases} \frac{2(x - z_j^{\min})}{(z_j^{\max} - z_j^{\min})(z_j^{\text{med}} - z_j^{\min})} & \text{for } z_j^{\min} \leq x < z_j^{\text{med}} \\ \frac{2(z_j^{\max} - x)}{(z_j^{\max} - z_j^{\min})(z_j^{\max} - z_j^{\text{med}})} & \text{for } z_j^{\text{med}} \leq x \leq z_j^{\max} \end{cases},$$

$$\mathbf{z} := [z_1, \dots, z_M]^T \in \mathbb{R}^M, \quad (3)$$

where \mathbf{z} is a full random sample from the distribution of \mathbf{Z} across all M dimensions, $z_j^{\min} = \{\min(\mathbf{Z}_{:,j})\}_{j=1}^M \in \mathbb{R}^M$ is the minimum \mathbf{Z} value for each embedding dimension, and $z_j^{\text{med}}, z_j^{\max} \in \mathbb{R}^M$ are the corresponding median and maximum \mathbf{Z} values. In practice, our Triangular distribution robustly covers both exponential- (ResNet) and Gaussian-shaped (CLIP) embedding distributions, naturally balancing between common and fringe embeddings (see Fig. 2).

We increase sample efficiency over $\mathbf{Z} \in \mathbb{R}^{N \times M}$ by re-

ducing its dimensionality to $\mathbb{R}^{N \times m}$ using

$$\begin{aligned} \mathbf{D} &:= [\mathbf{d}_1, \dots, \mathbf{d}_m] \in \mathbb{R}^{M \times m}, \\ \hat{\mathbf{Z}} &:= \mathbf{Z}\mathbf{D} \in \mathbb{R}^{N \times m}, \end{aligned} \quad (4)$$

where \mathbf{D} linearly maps \mathbf{Z} to m reduced embedding dimensions, $\mathbf{d} = [d_1, \dots, d_m]^T \in \mathbb{N}^m$ is a set of random indices chosen without replacement from $\{1, \dots, M\}$, and $\mathbf{1}_i$ is a one-hot vector with i -th element equal to 1. In plain words, we use \mathbf{D} to randomly select a subset of $m \leq M$ indices to represent \mathbf{Z} in a lower dimensional subspace $\hat{\mathbf{Z}}$. Notably, we also use Eq. (4) to reduce the dimension of random sampling $\mathbf{z} \in \mathbb{R}^M$ in Eq. (3) to find $\hat{\mathbf{z}} := \mathbf{z}\mathbf{D} \in \mathbb{R}^m$.

We quantify coverage for each random sample $\hat{\mathbf{z}}$ by finding the closest *existing* dataset example

$$\arg \min_i \|\hat{\mathbf{z}} - \hat{\mathbf{Z}}_i\|_1, \quad (5)$$

where we denote k as the solution to i in Eq. (5) and $\hat{\mathbf{Z}}_k$ is the dataset example closest to $\hat{\mathbf{z}}$. Finally, we quantify our importance score for coverage (s^c) as

$$\begin{aligned} s_i^c &:= \begin{cases} 1 & \text{for } i = k \\ 0 & \text{otherwise} \end{cases}, \\ \mathbf{s}^c &:= [s_1^c, \dots, s_N^c] \in \mathbb{R}^N, \end{aligned} \quad (6)$$

where s^c adds to the estimated embedding coverage value for dataset example k . We repeat our process of randomly sampling $\hat{\mathbf{z}}$ and subsequently adding coverage for the closest examples across many iterations to extend the coverage score across all examples in \mathbb{S} . Unlike random sampling, our coverage score rewards hard examples that individually occupy large, unique, low-density areas of the embedding space (see Fig. 1), which improves coreset selection.

Remarks on m : In Sec. 5 experiments, we choose $m = 2$ (s.t. $\mathbf{D} \in \mathbb{R}^{M \times 2}$) random embedding dimensions per sample $\hat{\mathbf{z}}$, which increases computational efficiency on large datasets while enabling $\binom{M}{2} \approx \frac{M^2}{2}$ unique 2-D embedding space slices of \mathbf{Z} over numerous sampling iterations.

4.3. Removing Embedding Space Redundancy

To avoid redundant coreset selection in the embedding space, we develop a redundancy estimate that operates subsequently to each coverage solution k in Eq. (5). Specifically, for each coverage example $\hat{\mathbf{Z}}_k$, we quantify redundancy for the set of $\mathbb{K} \in \mathbb{N}^\alpha$ nearest neighbors as

$$\mathbf{v}^r := \begin{cases} (\|\hat{\mathbf{Z}}_k - \hat{\mathbf{Z}}_i\|_1)^{-\beta} & \text{for } i \in \mathbb{K} \\ 0 & \text{otherwise} \end{cases}, \quad (7)$$

where exponent β determines the rate of penalty changes between $\hat{\mathbf{Z}}_k$ neighbors with varying distance $\|\hat{\mathbf{Z}}_k - \hat{\mathbf{Z}}_i\|_1$. We use $\mathbf{v}^r \in \mathbb{R}^N$ to define our redundancy score as

$$\mathbf{s}^r := \frac{\mathbf{v}^r}{\|\mathbf{v}^r\|_1}, \quad (8)$$

where $\|\mathbf{v}^r\|_1 \in \mathbb{R}$ normalizes $\mathbf{s}^r \in \mathbb{R}^N$ so that the coverage and redundancy scores for each sample iteration are balanced as $\|\mathbf{s}^c\|_1 = \|\mathbf{s}^r\|_1 = 1$.

Remarks on α, β : In Sec. 5 experiments, we choose $\alpha = 1,000$ to limit computation of Eq. (7) on large datasets while still reaching many examples per iteration, and we choose $\beta = 4$ to ensure that primarily the closest neighbors to each $\hat{\mathbf{Z}}_k$ are substantially estimated as redundant.

4.4. Pruning Procedure

Using the embedding sampling process for $\hat{\mathbf{z}}$ in Eq. (5) and subsequent coverage \mathbf{s}^c and \mathbf{s}^r scores, we define our final importance score $\mathbf{s} \in \mathbb{R}^N$ as

$$\mathbf{s} := \mathbf{s} + \sum_{t=1}^T \mathbf{s}_t^c(\hat{\mathbf{z}}_t) - \mathbf{s}_t^r(k_t), \quad (9)$$

where $\mathbf{s} = \{s_i \sim \mathcal{U}[0, 1]\}_{i=1}^N$ is a random initialization for each example, $\hat{\mathbf{z}}_t$ is the embedding space sample $\hat{\mathbf{z}}$ at iteration t with corresponding coverage score $\mathbf{s}_t^c(\hat{\mathbf{z}}_t)$, k_t is the example solution in Eq. (5) at iteration t with corresponding redundancy score $\mathbf{s}_t^r(k_t)$, and T is the total number of sample and score iterations. Notably, \mathbf{s} promotes inclusion of a few examples outside of our primary coverage and redundancy measures and each iteration t is independent, enabling us to parallelize and accelerate score computation.

Finally, after finding \mathbf{s} as our importance score to rank all examples in unlabeled dataset \mathbb{S} , we select the n examples with highest scores as our pruned coreset for model training.

For experiments in Sec. 5, we also use \mathbf{s} to weight the loss and gradient for model training using

$$\mathbf{w} = \frac{\mathbf{s} - \min(\mathbf{s})}{\max(\mathbf{s}) - \min(\mathbf{s})}, \quad (10)$$

where $\mathbf{w} = [w_1, \dots, w_N]^\top \in \mathbb{R}^N$, $w_i \in [0, 1]$, and the loss is scaled each batch by the mean w_i score corresponding to

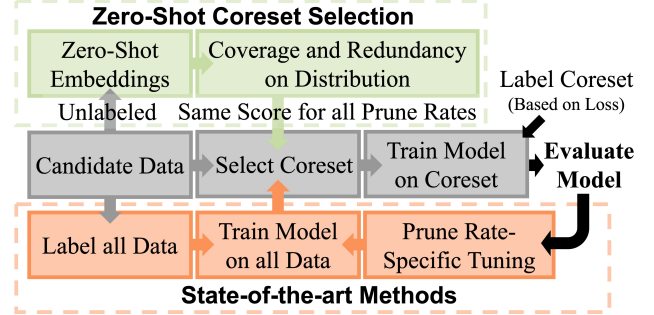


Figure 3. Coreset Selection Method Comparison.

the specific training examples in that batch. Basically, we already assign a value to each example for coreset selection and want to influence model training accordingly.

5. Evaluation

5.1. Experimental Setup

Datasets. We evaluate the effectiveness of Zero-Shot Coreset Selection (ZCore) on four image classification datasets: CIFAR10 [17], CIFAR100, ImageNet [9], and EuroSAT [15]. We compare the full training and coreset size across each dataset in Tab. 2. Notably, full dataset sizes span from 1.3 M to 2,700 examples and coreset sizes span from 896,817 to 270 examples (three orders of magnitude). EuroSAT has no explicit training set, so we create “four” datasets using 80/20, 40/60, 20/80, and 10/90 training/validation splits to experiment with dataset scale in the same distribution of satellite images.

Network Training. We use two different network models and training regimes to evaluate coresets. For CIFAR10, CIFAR100, and EuroSAT, we train a ResNet18 model on selected coresets for 200 epochs with a batch size of 128. For ImageNet, we alternatively train a ResNet32 model for 60 epochs with a batch size of 256. Following the protocol of [44], we use an SGD optimizer with momentum 0.9, weight decay 0.0005, and a learning rate of 0.1 that decays with the cosine annealing scheduler via PyTorch [28]. After model training, we use the model’s validation accuracy to quantitatively evaluate coreset selection performance.

ZCore & Baselines. We implement ZCore using the Sec. 4 formulation with constant parameter settings across all datasets and prune rates. We compare ZCore against the state-of-the-art using eight methods. ZCore is the only method that does not use ground truth labels and dataset training (see Fig. 3) aside from **Random**, which selects examples with uniform random sampling. **Entropy** selects examples with high entropy of predicted probabilities at the end of training [7]. **Forgetting** selects examples that change to being misclassified after correct classification the most times during training [37]. **EL2N** selects examples with

Table 2. Comparison of **full training and coreset size** across all datasets. Prune rate is the % of training data removed. ZCore uses constant parameter settings across all datasets and prune rates and, unlike label-based methods, removes labeling requirements from the full dataset.

Dataset	Scale	Number of Classes	Full Dataset Training Size	Coreset Size Across Prune Rates				
				30%	50%	70%	80%	90%
ImageNet	Large	1,000	1,281,167	896,817	640,584	384,350	256,233	128,117
CIFAR100	Medium	100	50,000	35,000	25,000	15,000	10,000	5,000
CIFAR10	Medium	10	50,000	35,000	25,000	15,000	10,000	5,000
EuroSAT80	Medium	10	21,600	15,120	10,800	6,480	4,320	2,160
EuroSAT40	Small	10	10,800	7,560	5,400	3,240	2,160	1,080
EuroSAT20	Small	10	5,400	3,780	2,700	1,620	1,080	540
EuroSAT10	Small	10	2,700	1,890	1,350	810	540	270

Table 3. Comparison of Unlabeled and Labeled coreset selection methods on **CIFAR10** and **CIFAR100**. Full dataset training on the ResNet18 model achieves 95.23% (CIFAR10) and 78.21% (CIFAR100) accuracy. Prune rate is the % of training data removed. “Rel. Rand.” is Mean accuracy across all prune rates on both datasets relative to Random. ZCore and TDDS prune selections outperform all other methods and Random on both datasets. A corresponding results plot is provided in the supplementary material.

	CIFAR10					CIFAR100					
Prune Rate	30%	50%	70%	80%	90%	30%	50%	70%	80%	90%	Mean Rel. Rand.
Unlabeled Coreset Selection without Training											
ZCore	94.58 ± 0.09	93.46 ± 0.16	90.97 ± 0.17	89.06 ± 0.33	84.18 ± 0.21	76.04 ± 0.15	72.87 ± 0.18	65.92 ± 0.15	61.92 ± 0.39	52.11 ± 0.66	78.11 $+1.34$
Random	94.58 ± 0.04	93.38 ± 0.17	90.61 ± 0.44	88.87 ± 0.47	83.77 ± 0.26	75.53 ± 0.04	71.95 ± 0.16	64.59 ± 0.32	57.79 ± 0.24	46.68 ± 1.07	76.78 $+0.00$
Labeled Coreset Selection with Training-based Pruning											
TDDS [44] CVPR 2024	95.47 ± 0.06	95.21 ± 0.04	93.03 ± 0.25	91.30 ± 0.25	85.46 ± 0.21	77.56 ± 0.06	74.04 ± 0.34	67.78 ± 0.44	63.01 ± 0.12	54.51 ± 0.22	79.74 $+2.96$
Moderate [41] ICLR 2023	93.96 ± 0.06	92.34 ± 0.09	89.71 ± 0.14	87.75 ± 0.27	83.61 ± 0.24	74.60 ± 0.10	70.29 ± 0.31	62.81 ± 0.08	56.52 ± 0.37	41.82 ± 1.12	75.34 -1.43
Entropy [7] ICLR 2020	94.45 ± 0.07	91.90 ± 0.16	86.24 ± 0.26	83.49 ± 0.21	72.06 ± 0.81	72.39 ± 0.20	64.44 ± 0.36	50.73 ± 0.86	42.86 ± 0.25	29.56 ± 0.54	68.81 -7.96
Forgetting [37] ICLR 2019	95.45 ± 0.24	95.05 ± 0.05	89.14 ± 2.04	76.18 ± 3.18	45.87 ± 1.87	77.38 ± 0.09	70.76 ± 0.40	49.92 ± 0.28	38.42 ± 1.13	25.82 ± 0.52	66.40 -10.38
Dyn-Unc [14] CVPR WS '24	95.08 ± 0.02	94.03 ± 0.14	89.40 ± 0.13	79.76 ± 1.09	37.12 ± 1.12	73.36 ± 0.10	65.90 ± 0.25	50.16 ± 0.47	39.19 ± 0.27	15.20 ± 0.41	63.92 -12.86
AUM [30] NeurIPS 2020	95.44 ± 0.09	95.19 ± 0.09	91.19 ± 0.63	69.60 ± 3.11	34.74 ± 0.11	77.35 ± 0.18	68.17 ± 0.52	31.69 ± 0.34	18.43 ± 0.47	9.29 ± 0.27	59.11 -17.67
EL2N [29] NeurIPS 2021	95.43 ± 0.10	95.06 ± 0.04	86.69 ± 1.71	68.64 ± 3.70	31.89 ± 1.51	76.89 ± 0.31	67.57 ± 0.15	36.45 ± 1.36	17.31 ± 0.33	9.10 ± 0.69	58.50 -18.27

high gradient magnitude using the L2 norm of error vectors [29]. **AUM** selects examples with high area under the margin, i.e., the probability gap between the target class and the next largest class across all epochs [30]. **Moderate** selects examples closest to the median class value in the full dataset trained model embedding space [41]. **Dyn-Unc** selects examples with high target class probability variance during training [14]. **TDDS** selects examples with high projected gradient variance across many epochs [44].

5.2. Coreset Performance Comparison

We provide coreset selection results for CIFAR10 and CIFAR100 in Tab. 3, which demonstrates coreset selection on two medium-sized datasets. Relative to CIFAR10, CIFAR100 is more challenging with an order of magnitude more classes. Across both datasets, ZCore achieves the best performance over all label- and training-based meth-

ods at all prune rates, with the exception of TDDS, which is a label- and training-based method. Notably, ZCore and TDDS are the only methods outperforming Random, with the largest relative performance gaps between methods occurring at high prune rates.

We provide coreset selection results for ImageNet in Tab. 4, which demonstrates coreset selection at a large scale. Overall, ZCore and TDDS coreset selections outperform all other methods. Notably, ZCore selects the best performing coreset at the 90% prune rate without using any labels, which removes label requirements for 1.15 million images.

We plot coreset selection results for all EuroSAT dataset splits in Fig. 4, which demonstrates coreset selection for the three leading methods at a much smaller scale. Except for the 90% prune rate on small datasets, ZCore cuts much of the performance gap between unlabeled Random selection and label- and training-based TDDS. For 90% prune

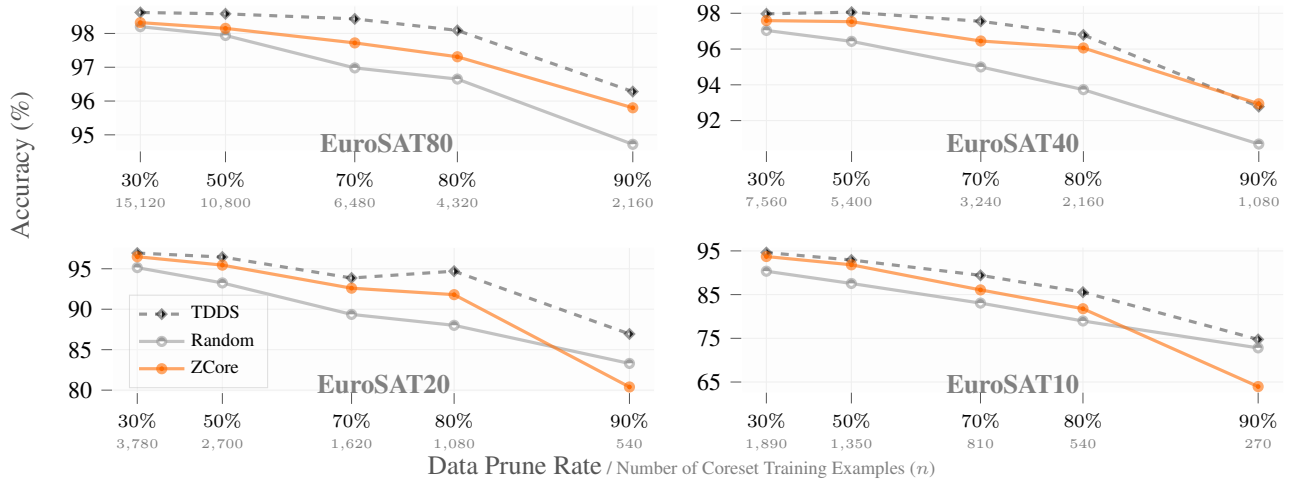


Figure 4. Comparison of Unlabeled (solid lines) and Labeled (dashed) coreset selection methods on 80/20, 40/60, 20/80, and 10/90 training/validation splits of **EuroSAT**. Dashed line indicates labeled coreset selection with training-based pruning. x -axis is in log scale for Number of Coreset Training Examples. ZCore and TDDS prune selections outperform the mean accuracy of Random on all EuroSAT splits. A corresponding results table is provided in the supplementary material.

Table 4. Comparison of Unlabeled and Labeled coreset selection methods on **ImageNet**. Full dataset training on the ResNet32 model training achieves 73.54% accuracy. ZCore has the best 90% prune rate performance despite using unlabeled data. A corresponding results plot is provided in the supplementary material.

Prune Rate	70%	80%	90%	Mean / Rel. Rand.
Unlabeled Coreset Selection without Training				
ZCore	64.43	61.31	53.99	59.91 $+0.72$
Random	64.19	60.76	52.63	59.19 $+0.00$
Labeled Coreset Selection with Training-based Pruning				
TDDS [44]	64.69	62.56	53.91	60.39 $+1.19$
Forgetting [37]	64.29	62.01	52.14	59.48 $+0.29$
Moderate [41]	64.04	61.35	52.45	59.28 $+0.09$
Entropy [7]	62.34	56.80	43.39	54.18 -5.02

rates, ZCore outperforms TDDS on EuroSAT40 but has a lower accuracy than TDDS and Random on EuroSAT20 and EuroSAT10, where the pruned coresets only have 540 and 270 training examples. Notably, unlike TDDS, ZCore is currently using constant parameter settings across all prune rates. On the other hand, ZCore small dataset performance improves with alternative settings (e.g., reducing the number of nearest neighbors for redundancy in Eq. (7)), which we will address in future work.

5.3. Ablation Study

We provide ZCore ablative results in Tab. 5. When using a single model to generate our embedding space (\mathbf{Z}), ResNet18 outperforms CLIP, but neither perform as well as the standard concatenated setting. We also test a DINOv2 ViT-B-14 model [25], which shows that ZCore maintains

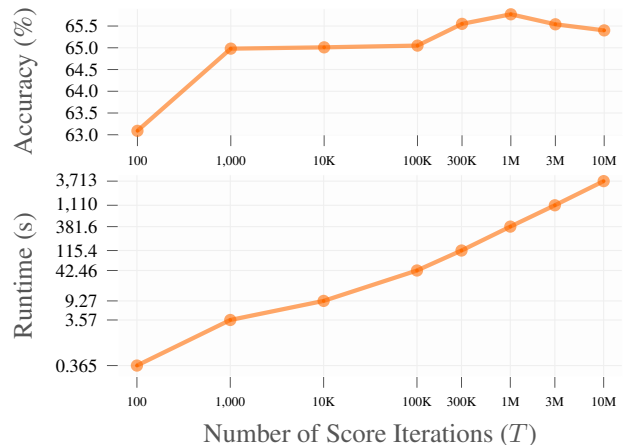


Figure 5. Comparison of number of score iterations vs. accuracy (top) and **runtime** (bottom) on CIFAR100 with ResNet18. Accuracy is mean across 30%, 50%, 70%, 80%, and 90% prune rates over five repeat trials. The accuracy peaks at 1 M iterations then converges on a slightly lower accuracy. Runtime experiments measure coreset selection times using a M3 Max-equipped laptop.

near full performance even with a self-supervised zero-shot embedding space. Gaussian sampling (\mathbf{z}) outperforms uniform but does not match Triangular performance. Given the narrow performance gap between Triangular and Gaussian sampling, we postulate that exploring additional sampling strategies is a promising area for future work. Decreasing or increasing the sample dimension of the embedding space (m) leads to lower performance, with high-dimension samples performing worst. We postulate this performance drop occurs because the current distance measure in Eq. (5) is less meaningful in higher-dimensional space [27].

Table 5. Comparison of **ZCore** ablations on CIFAR 100 with ResNet18. Accuracy is mean across 30%, 50%, 70%, 80%, and 90% prune rates over five repeat trials. “ResNet18, CLIP” is a concatenated zero-shot embedding space that uses both foundation models off-the-shelf.

Ablation	Zero-shot	Sampling		Redundancy		Use Full	CIFAR100
	Embedding Model	Distribution	Dimensions	Neighbors	Distance	Score	Accuracy
Full Method (ZCore)	ResNet18, CLIP	Triangular	2	1,000	4	Yes	65.77
Embedding Space (Z)	ResNet18 [13]	Triangular	2	1,000	4	Yes	65.52
	CLIP [31]	Triangular	2	1,000	4	Yes	64.84
	DINOv2 [25]	Triangular	2	1,000	4	Yes	65.61
Sampling Distribution (z)	ResNet18, CLIP	Gaussian	2	1,000	4	Yes	65.75
	ResNet18, CLIP	Uniform	2	1,000	4	Yes	64.84
Number of Dimensions (m) per Embedding Sample	ResNet18, CLIP	Triangular	1	1,000	4	Yes	64.59
	ResNet18, CLIP	Triangular	3	1,000	4	Yes	65.10
	ResNet18, CLIP	Triangular	10	1,000	4	Yes	63.27
	ResNet18, CLIP	Triangular	100	1,000	4	Yes	62.20
Number of Nearest	ResNet18, CLIP	Triangular	2	100	4	Yes	65.68
Neighbors (α)	ResNet18, CLIP	Triangular	2	10,000	4	Yes	65.72
Distance Penalty	ResNet18, CLIP	Triangular	2	1,000	3	Yes	65.64
Exponent (β)	ResNet18, CLIP	Triangular	2	1,000	5	Yes	65.74
Random Coverage Sample (k)	NA	NA	NA	1,000	4	No	64.74
No Redundancy Score (s^R)	ResNet18, CLIP	Triangular	2	NA	NA	No	61.71
No Random Initialization (s)	ResNet18, CLIP	Triangular	2	1,000	4	No	65.66
No Score Loss Weight (w)	ResNet18, CLIP	Triangular	2	1,000	4	No	63.53

We also test multiple redundancy score settings (α, β) and find that ZCore performance is robust to these parameter changes. Changing the score selection to use a uniformly random coverage sample k decreases performance, which validates our design choice to focus coverage selection on embedding examples that occupy larger, lower-density areas. Removing redundancy score (s^R) decreases performance more substantially than any other ablative configuration, which validates our design choice to penalize nearest neighbors in the embedding space to reduce redundancy. Finally, removing random initialization (s) or the score loss weight w from model training decreases performance.

We plot the runtime and accuracy performance of ZCore over a wide range of score iterations in Fig. 5. The largest accuracy increase occurs when the coverage and redundancy score iterations (T) increase from 100 to 1,000, at which point, with the redundancy score reaching 1,000 neighbors per iteration, the score likely reaches most of the 50,000 CIFAR100 candidate training examples. Notably, the standard ZCore configuration ($T = 1M$) runtime takes less than 400 s on a standard laptop, which, in addition to being able to select coresets for unlabeled data, makes ZCore a computationally efficient alternative to label- and training-based coreset selection methods.

6. Conclusion

We motivate and develop a method for *unlabeled* coreset selection, which, relative to label-based methods, uniquely enables data- and label-efficient deep learning. Further-

more, our approach requires less computation than state-of-the-art methods by removing training requirements on the data being considered for selection. Instead, our approach uses zero-shot embeddings that can be generated by a variety of existing foundation models, including those trained with self-supervision.

We evaluate our method against the state-of-the-art using eight baselines across four datasets, ranging from initial datasets of over a million images all the way down to pruned coresets of 270 training images. In these experiments, our method outperforms all others save one, which requires full ground truth labels and model training on the initial dataset prior to coreset selection. However, our method alone does not use labels or dataset training, making it more efficient for coreset selection at the scale of current deep learning research. From these results, our method establishes a new state-of-the-art for coreset selection.

In future work, to further improve performance on very small datasets, we will develop a sampling scheme that automatically determines the number of samples and nearest neighbors for redundancy scoring. In addition to the coverage and redundancy scores in this paper, we postulate that there are many more unlabeled features that can quantify coreset value for individual candidate examples. Furthermore, since there is no domain-specific limitation to our method, we will explore how it and the general coreset selection problem are applicable in other domains like point cloud and natural language and other problems like object detection and segmentation.

References

- [1] Dario Amodei, Danny Hernandez, GirishSastry, Jack Clark, Greg Brockman, and Ilya Sutskever. Ai and compute. 2018. 1
- [2] Jordan T. Ash, Chicheng Zhang, Akshay Krishnamurthy, John Langford, and Alekh Agarwal. Deep batch active learning by diverse, uncertain gradient lower bounds. In *International Conference on Learning Representations (ICLR)*, 2020. 2
- [3] Olivier Bachem, Mario Lucic, and Andreas Krause. Coresets for nonparametric estimation - the case of dp-means. In *Proceedings of the 32nd International Conference on Machine Learning (ICML)*, 2015. 2
- [4] J. Bernard, M. Hutter, M. Zeppelzauer, D. Fellner, and M. Sedlmair. Comparing visual-interactive labeling with active learning: An experimental study. *IEEE Transactions on Visualization and Computer Graphics*, 2018. 2
- [5] George Cazenavette, Tongzhou Wang, Antonio Torralba, Alexei A. Efros, and Jun-Yan Zhu. Dataset distillation by matching training trajectories. In *Proceedings of the IEEE/CVF Conference on Computer Vision and Pattern Recognition (CVPR) Workshops*, 2022. 2
- [6] Gui Citovsky, Giulia DeSalvo, Claudio Gentile, Lazaros Karydas, Anand Rajagopalan, Afshin Rostamizadeh, and Sanjiv Kumar. Batch active learning at scale. In *Advances in Neural Information Processing Systems (NeurIPS)*, 2021. 2
- [7] Cody Coleman, Christopher Yeh, Stephen Mussmann, Baharan Mirzasoleiman, Peter Bailis, Percy Liang, Jure Leskovec, and Matei Zaharia. Selection via proxy: Efficient data selection for deep learning. In *International Conference on Learning Representations (ICLR)*, 2020. 5, 6, 7
- [8] Marius Cordts, Mohamed Omran, Sebastian Ramos, Timo Rehfeld, Markus Enzweiler, Rodrigo Benenson, Uwe Franke, Stefan Roth, and Bernt Schiele. The cityscapes dataset for semantic urban scene understanding. In *Proceedings of the IEEE Conference on Computer Vision and Pattern Recognition (CVPR)*, 2016. 2
- [9] Jia Deng, Wei Dong, Richard Socher, Li-Jia Li, Kai Li, and Li Fei-Fei. Imagenet: A large-scale hierarchical image database. In *IEEE Conference on Computer Vision and Pattern Recognition (CVPR)*, 2009. 5
- [10] Alexey Dosovitskiy, Lucas Beyer, Alexander Kolesnikov, Dirk Weissenborn, Xiaohua Zhai, Thomas Unterthiner, Mostafa Dehghani, Matthias Minderer, Georg Heigold, Sylvain Gelly, Jakob Uszkoreit, and Neil Houlsby. An image is worth 16x16 words: Transformers for image recognition at scale. In *International Conference on Learning Representations (ICLR)*, 2021. 1
- [11] Thomas Elsken, Jan Hendrik Metzen, and Frank Hutter. Neural architecture search: A survey. *Journal of Machine Learning Research*, 2019. 1
- [12] Dan Feldman, Matthew Faulkner, and Andreas Krause. Scalable training of mixture models via coresets. In *Advances in Neural Information Processing Systems (NeurIPS)*, 2011. 1, 2
- [13] Kaiming He, Xiangyu Zhang, Shaoqing Ren, and Jian Sun. Deep residual learning for image recognition. In *IEEE Conference on Computer Vision and Pattern Recognition (CVPR)*, 2016. 4, 8
- [14] Muyang He, Shuo Yang, Tiejun Huang, and Bo Zhao. Large-scale dataset pruning with dynamic uncertainty. In *IEEE/CVF Conference on Computer Vision and Pattern Recognition (CVPR) Workshops*, 2024. 3, 6
- [15] Patrick Helber, Benjamin Bischke, Andreas Dengel, and Damian Borth. Eurosat: A novel dataset and deep learning benchmark for land use and land cover classification. *IEEE Journal of Selected Topics in Applied Earth Observations and Remote Sensing*, 2019. 5
- [16] Suyog Dutt Jain and Kristen Grauman. Predicting sufficient annotation strength for interactive foreground segmentation. In *IEEE International Conference on Computer Vision (ICCV)*, 2013. 2
- [17] Alex Krizhevsky. Learning multiple layers of features from tiny images. 2009. 5
- [18] Alex Krizhevsky, Ilya Sutskever, and Geoffrey E Hinton. Imagenet classification with deep convolutional neural networks. In *Advances in Neural Information Processing Systems (NeurIPS)*, 2012. 1
- [19] Liam Li and Ameet Talwalkar. Random search and reproducibility for neural architecture search. In *Proceedings of The 35th Uncertainty in Artificial Intelligence Conference*, 2020. 1
- [20] Jonathan Lorraine, Paul Vicol, and David Duvenaud. Optimizing millions of hyperparameters by implicit differentiation. In *Proceedings of the Twenty Third International Conference on Artificial Intelligence and Statistics*, 2020. 1
- [21] Dougal Maclaurin, David Duvenaud, and Ryan Adams. Gradient-based hyperparameter optimization through reversible learning. In *Proceedings of the 32nd International Conference on Machine Learning (ICML)*, 2015. 1
- [22] Andrew McCallum and Kamal Nigam. Employing EM and pool-based active learning for text classification. In *International Conference on Machine Learning (ICML)*, 1998. 2
- [23] Nicholas Metropolis and Stanislaw Ulam. The monte carlo method. *Journal of the American Statistical Association*, 44 (247):335–341, 1949. 4
- [24] B. E. Moore and J. J. Corso. Fiftyone. <https://github.com/voxel51/fiftyone>, 2020. 1
- [25] Maxime Oquab, Timothée Darcet, Théo Moutakanni, Huy V. Vo, Marc Szafraniec, Vasil Khalidov, Pierre Fernandez, Daniel HAZIZA, Francisco Massa, Alaaeldin El-Nouby, Mido Assran, Nicolas Ballas, Wojciech Galuba, Russell Howes, Po-Yao Huang, Shang-Wen Li, Ishan Misra, Michael Rabbat, Vasu Sharma, Gabriel Synnaeve, Hu Xu, Herve Jegou, Julien Mairal, Patrick Labatut, Armand Joulin, and Piotr Bojanowski. DINOv2: Learning robust visual features without supervision. *Transactions on Machine Learning Research (TMLR)*, 2024. 7, 8
- [26] Dongmin Park, Seola Choi, Doyoung Kim, Hwanjun Song, and Jae-Gil Lee. Robust data pruning under label noise via maximizing re-labeling accuracy. In *Advances in Neural Information Processing Systems (NeurIPS)*, 2023. 2
- [27] Jae Hyeon Park, Gyoomin Lee, Seunggi Park, and Sung In Cho. Not all classes stand on same embeddings: Calibrating

- a semantic distance with metric tensor. In *Proceedings of the IEEE/CVF Conference on Computer Vision and Pattern Recognition (CVPR)*, 2024. 7
- [28] Adam Paszke, Sam Gross, Francisco Massa, Adam Lerer, James Bradbury, Gregory Chanan, Trevor Killeen, Zeming Lin, Natalia Gimelshein, Luca Antiga, Alban Desmaison, Andreas Kopf, Edward Yang, Zachary DeVito, Martin Raison, Alykhan Tejani, Sasank Chilamkurthy, Benoit Steiner, Lu Fang, Junjie Bai, and Soumith Chintala. Pytorch: An imperative style, high-performance deep learning library. In *Advances in Neural Information Processing Systems (NeurIPS)*, 2019. 5
- [29] Mansheej Paul, Surya Ganguli, and Gintare Karolina Dziugaite. Deep learning on a data diet: Finding important examples early in training. In *Advances in Neural Information Processing Systems (NeurIPS)*, 2021. 6
- [30] Geoff Pleiss, Tianyi Zhang, Ethan Elenberg, and Kilian Q Weinberger. Identifying mislabeled data using the area under the margin ranking. In *Advances in Neural Information Processing Systems (NeurIPS)*, 2020. 6
- [31] Alec Radford, Jong Wook Kim, Chris Hallacy, Aditya Ramesh, Gabriel Goh, Sandhini Agarwal, Girish Sastry, Amanda Askell, Pamela Mishkin, Jack Clark, Gretchen Krueger, and Ilya Sutskever. Learning transferable visual models from natural language supervision. In *Proceedings of the 38th International Conference on Machine Learning (ICML)*, 2021. 4, 8
- [32] Aditya Ramesh, Prafulla Dhariwal, Alex Nichol, Casey Chu, and Mark Chen. Hierarchical text-conditional image generation with clip latents. *arXiv preprint arXiv:2204.06125*, 2022. 1
- [33] Ozan Sener and Silvio Savarese. Active learning for convolutional neural networks: A core-set approach. In *International Conference on Learning Representations (ICLR)*, 2018. 2, 3
- [34] Burr Settles. Active learning. *Synthesis Lectures on Artificial Intelligence and Machine Learning*, 2012. 2
- [35] Ben Sorscher, Robert Geirhos, Shashank Shekhar, Surya Ganguli, and Ari Morcos. Beyond neural scaling laws: beating power law scaling via data pruning. In *Advances in Neural Information Processing Systems (NeurIPS)*, 2022. 2, 3
- [36] Haoru Tan, Sitong Wu, Fei Du, Yukang Chen, Zhibin Wang, Fan Wang, and Xiaojuan Qi. In *Advances in Neural Information Processing Systems (NeurIPS)*, 2023. 2
- [37] Mariya Toneva, Alessandro Sordoni, Remi Tachet des Combes, Adam Trischler, Yoshua Bengio, and Geoffrey J. Gordon. An empirical study of example forgetting during deep neural network learning. In *International Conference on Learning Representations (ICLR)*, 2019. 2, 5, 6, 7
- [38] Kai Wang, Bo Zhao, Xiangyu Peng, Zheng Zhu, Shuo Yang, Shuo Wang, Guan Huang, Hakan Bilen, Xinchao Wang, and Yang You. Cafe: Learning to condense dataset by aligning features. In *Proceedings of the IEEE/CVF Conference on Computer Vision and Pattern Recognition (CVPR)*, 2022. 2
- [39] Kai Wei, Rishabh Iyer, and Jeff Bilmes. Submodularity in data subset selection and active learning. In *Proceedings of the 32nd International Conference on Machine Learning (ICML)*, 2015. 2
- [40] Max Welling. Herding dynamical weights to learn. In *Proceedings of the 26th Annual International Conference on Machine Learning (ICML)*, 2009. 2
- [41] Xiaobo Xia, Jiale Liu, Jun Yu, Xu Shen, Bo Han, and Tongliang Liu. Moderate coreset: A universal method of data selection for real-world data-efficient deep learning. In *International Conference on Learning Representations (ICLR)*, 2023. 2, 3, 6, 7
- [42] Shuo Yang, Zeke Xie, Hanyu Peng, Min Xu, Mingming Sun, and Ping Li. Dataset pruning: Reducing training data by examining generalization influence. In *The Eleventh International Conference on Learning Representations (ICLR)*, 2023. 2
- [43] Ruonan Yu, Songhua Liu, and Xinchao Wang. Dataset distillation: A comprehensive review. *IEEE Transactions on Pattern Analysis and Machine Intelligence (TPAMI)*, 2024. 2
- [44] Xin Zhang, Jiawei Du, Yunsong Li, Weiyang Xie, and Joey Tianyi Zhou. Spanning training progress: Temporal dual-depth scoring (tdds) for enhanced dataset pruning. In *IEEE/CVF Conference on Computer Vision and Pattern Recognition (CVPR)*, 2024. 2, 3, 5, 6, 7
- [45] Bo Zhao and Hakan Bilen. Dataset condensation with differentiable siamese augmentation. In *Proceedings of the 38th International Conference on Machine Learning (ICML)*, 2021. 2
- [46] Bo Zhao and Hakan Bilen. Dataset condensation with distribution matching. In *Proceedings of the IEEE/CVF Winter Conference on Applications of Computer Vision (WACV)*, 2023. 1, 2
- [47] Bo Zhao, Konda Reddy Mopuri, and Hakan Bilen. Dataset condensation with gradient matching. In *International Conference on Learning Representations (ICLR)*, 2021. 2
- [48] Haizhong Zheng, Rui Liu, Fan Lai, and Atul Prakash. Coverage-centric coreset selection for high pruning rates. In *The Eleventh International Conference on Learning Representations (ICLR)*, 2023. 2, 3

Supplementary Material

Zero-Shot Coreset Selection: Efficient Pruning for Unlabeled Data

Reproducibility Statement. We provide detailed experimental settings in Secs. 4 and 5. We generate all ZCore experimental results from a single attempt of five consecutive trials with the exception of ImageNet, which is from a single attempt of one trial. Our code is publicly available at <https://github.com/voxel51/zcore>.

Additional Figures & Tables. To supplement the evaluation in Sec. 5, we provide additional Figures and Tables. We plot coreset selection results for ImageNet in Fig. 6, which demonstrates coreset selection at a large scale. We plot coreset selection results for CIFAR10 and CIFAR100 in Fig. 7, which demonstrates coreset selection for two medium-sized datasets. We provide coreset selection results for all EuroSAT dataset splits in Tab. 6, which demonstrates coreset selection for the three leading methods at a much smaller scale. We plot DINOv2 model embeddings and corresponding sample distributions in Fig. 8.



Figure 6. Comparison of Unlabeled (solid lines) and Labeled (dashed lines) coreset selection methods on **ImageNet**. Dashed line indicates labeled coreset selection with training-based pruning. x -axis is in log scale for Number of Coreset Training Examples. ZCore achieves best 90% prune rate performance without using label- or training-based prune selection. A corresponding results table is provided in Tab. 4 of the main paper.

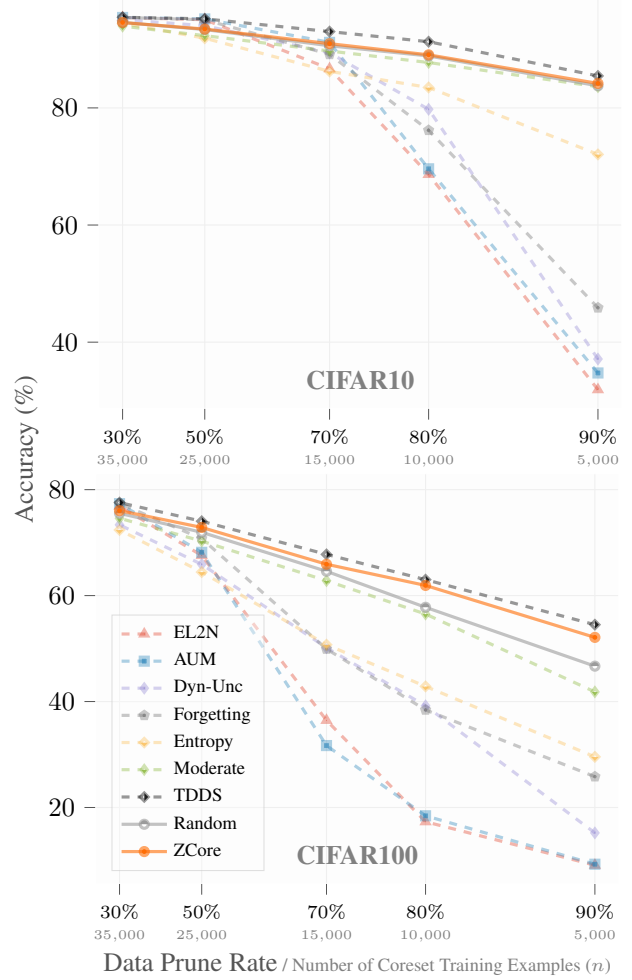


Figure 7. Comparison of Unlabeled (solid lines) and Labeled (dashed lines) coreset selection methods on **CIFAR10** and **CIFAR100**. Dashed line indicates labeled coreset selection with training-based pruning. x -axis is in log scale for Number of Coreset Training Examples. Notably, ZCore and TDDS are the only methods outperforming Random, with the largest relative performance gaps between methods occurring at high prune rates. A corresponding results table is provided in Tab. 3 of the main paper.

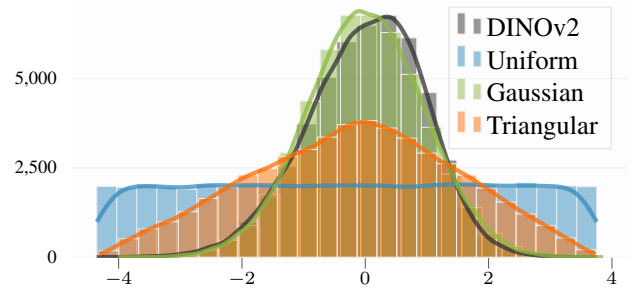


Figure 8. Comparison of real embedding data (gray) and **sampling techniques**. DINOv2 is the first dimension embeddings for 50,000 CIFAR100 train set examples, while each corresponding distribution type is sampled 50,000 times. Corresponding plots for ResNet18 and CLIP are provided in Fig. 2 of the main paper.

Table 6. Comparison of Unlabeled and Labeled coreset selection methods on different sized splits of **EuroSAT**. Full dataset training on the ResNet18 model achieves 98.59% (EuroSAT80), 98.20% (EuroSAT40), 98.59% (EuroSAT20), and 93.64% (EuroSAT10) accuracy. “Rel. Rand.” is Mean accuracy across all prune rates relative to Random. “EuroSAT All” is Mean accuracy for all EuroSAT splits. ZCore and TDDS prune selections outperform the mean accuracy of Random on all EuroSAT splits. Notably, the EuroSAT 10 90% prune rate coreset has only 270 training examples. A corresponding results plot is provided in Fig. 4 of the main paper.

Prune Method	Coreset Selection Requirements	Data Prune Rate / Number of Examples					Mean Rel. Rand.
		30%	50%	70%	80%	90%	
EuroSAT All							
ZCore	Unlabeled Data	96.53	95.74	93.21	91.74	83.27	92.10 +1.14
Random	Unlabeled Data	94.56	92.91	89.80	87.88	83.61	90.96 +0.00
TDDS CVPR 2024	Full Training on Labeled Data	96.93	96.35	94.55	93.56	87.80	93.96 + 3.01
EuroSAT80 (21,600)							
ZCore	Unlabeled Data	98.32 ±0.08	98.15 ±0.13	97.72 ±0.13	97.31 ±0.17	95.80 ±0.18	97.46 +0.56
Random	Unlabeled Data	98.20 ±0.11	97.94 ±0.10	96.98 ±0.17	96.65 ±0.29	94.72 ±0.49	96.90 +0.00
TDDS CVPR 2024	Full Training on Labeled Data	98.62 ±0.05	98.58 ±0.11	98.43 ±0.03	98.09 ±0.10	96.28 ±0.11	98.00 +1.10
EuroSAT40 (10,800)							
ZCore	Unlabeled Data	97.59 ±0.05	97.53 ±0.16	96.45 ±0.12	96.06 ±0.19	92.94 ±0.55	96.11 +1.54
Random	Unlabeled Data	97.04 ±0.07	96.43 ±0.37	95.00 ±0.67	93.73 ±0.58	90.69 ±0.53	94.58 +0.00
TDDS CVPR 2024	Full Training on Labeled Data	97.97 ±0.09	98.06 ±0.06	97.55 ±0.08	96.79 ±0.16	92.78 ±0.27	96.63 +2.05
EuroSAT20 (5,400)							
ZCore	Unlabeled Data	96.49 ±0.16	95.45 ±0.22	92.60 ±0.29	91.80 ±0.70	80.39 ±3.91	91.35 +1.53
Random	Unlabeled Data	95.14 ±0.32	93.25 ±0.59	89.36 ±0.54	88.01 ±0.22	83.30 ±0.73	89.81 +0.00
TDDS CVPR 2024	Full Training on Labeled Data	96.94 ±0.10	96.45 ±0.07	93.86 ±0.56	94.70 ±0.35	86.94 ±0.55	93.78 +3.97
EuroSAT10 (2,700)							
ZCore	Unlabeled Data	93.71 ±0.23	91.82 ±0.23	86.08 ±1.16	81.77 ±2.68	63.96 ±2.76	83.47 +0.92
Random	Unlabeled Data	90.35 ±0.64	87.55 ±0.67	83.06 ±1.61	78.97 ±1.88	72.81 ±2.25	82.55 +0.00
TDDS CVPR 2024	Full Training on Labeled Data	94.62 ±0.09	92.92 ±0.33	89.41 ±0.52	85.56 ±0.67	74.74 ±2.02	87.45 +4.90